Available online at www.sciencedirect.com
SCIENCE DIRECT®
Biochemical and Biophysical Research Communications 305 (2003) 1024–1033
BBRC
www.elsevier.com/locate/ybbrc

Permeability and gating properties of human connexins 26 and 30 expressed in HeLa cells

Martina Beltramello,[a,b] Massimiliano Bicego,[c] Valeria Piazza,[a,b] Catalin D. Ciubotaru,[a,b] Fabio Mammano,[a,b,*] and Paola D'Andrea[c]

[a] *Venetian Institute of Molecular Medicine (VIMM), Padova University, via G. Orus 2, Padua 35129, Italy*
[b] *Istituto Nazionale di Fisica della Materia (INFM) and Dipartimento di Fisica "G.Galilei," Padova University, via Marzolo 8, Padua 35131, Italy*
[c] *Department of Biochemistry, Trieste University, via L. Giorgeri, Trieste 34100, Italy*

Received 23 April 2003

Abstract

Human connexins 26 and 30 were expressed either through the bicistronic pIRES-EGFP expression vector or as EYFP-tagged chimeras. When transiently transfected in communication-incompetent HeLa cells, hCx26–pIRES transfectants were permeable to dyes up to 622 Da, but were significantly less permeable to 759 Da molecules. Under the same conditions, permeability of hCx26–EYFP fusion products was comparable to that of hCx26–pIRES, but with significant increase in diffusion at 759 Da, possibly as a consequence of having selected large fluorescent junctional plaques. Dye transfer was limited to 457 Da in hCx30–EYFP transfectants. When reconstructed from confocal serial sections, fluorescent plaques formed by hCx26–EYFP and hCx30–EYFP appeared irregular, often with long protrusions or deep invagination. Similar plaques were observed following immunostaining both in cells transfected with hCx26–pIRES and in HeLa cells stably transfected with mouse Cx26. Tissue conductance (Tg_j) displayed significantly smaller values (28.8 ± 1.8 nS) for stably transfected mCx26 than transiently transfected hCx26 (43.5 ± 3.3 nS). These differences reflected in distinct functional dependence of normalized junctional conductance (G_j) on transjunctional voltage (V_j). The half-activation voltage for G_j was close to ± 95 and ± 58 mV in mCx26 and hCx26, respectively. The corresponding parameters for hCx30 transfectants were $Tg_j = 45.2 \pm 3.5$ nS and $V_0 = \pm 34$ mV. These results highlight unexpected differences between mCx26 and hCx26 in this expression system, reinforce the concept that channel permeability may be related to Cx level expression, and indicate that fusion of hCx30 to GFP colour mutants produces channels that are suitable for permeability and gating studies.

Keywords: Gap junctions; Deafness; Dye transfer; Dual patch clamp; Conductance; Molecular cloning; Fusion proteins; GFP mutants; Fluorescence; Confocal microscopy

The recent discovery of genetic diseases associated with mutations in six connexin genes has validated the view that gap junction-dependent intercellular signalling fulfils a crucial role in coordinating several aspects of tissue homeostasis. For example, mutations in Cx32 cause an X-linked form of Charcot–Marie–Tooth disease, a peripheral neuropathy [1], whereas mutations in either Cx46 or Cx50 result in autosomal dominant cataracts [2,3]. Recently, three connexins (Cx26, Cx30, or Cx31) have been identified as candidate genes for both syndromic and nonsyndromic deafness, as well as for different skin disorders [4–8].

In principle, Cx mutations might affect cell function in a number of ways; for instance, by altering protein expression levels, their trafficking and targeting to the plasma membrane, as well as the control of biophysical properties of the junctional channel (e.g., voltage- and/or chemical-gating or channel permeability to second messengers). Several missense mutations that impair protein expression and/or maturation have been described for Cx26, Cx30, and Cx31 [9–14]. Other mutated Cx proteins appear normally routed to the plasma membrane, but fail to sustain the intercellular transfer of fluorescent molecules, suggesting molecular defects

* Corresponding author. Fax: +39-049-7923-250.
E-mail address: fabio.mammano@unipd.it (F. Mammano).

0006-291X/03/$ - see front matter © 2003 Elsevier Science (USA). All rights reserved.
doi:10.1016/S0006-291X(03)00868-4

that alter either channel gating or its permeability [10,12].

Fusion proteins consisting of Cx with EGFP attached to its carboxyl terminus (Cx-EGFP) have been employed for functional studies of disease-associated Cx30 and Cx31 mutations [12,13]. Here, we took advantage of the bicistronic pIRES-EGFP plasmid (Clontech), which contains the internal ribosome entry site (IRES) of the encephalomyocarditis virus between the multiple cloning site and the EGFP-coding region. This permits both the gene of interest and EGFP to be translated from a single bicistronic mRNA, allowing an efficient selection of transfected cells [10,15,16].

Both approaches rely on the assumption that transiently expressed Cxs retain the physiological properties displayed in vivo. However, transient transfection often results in over-expression of the protein of interest. Moreover, the fusion of GFP and its colour mutants to the carboxyl-terminus of Cx proteins could, in principle, alter the molecular properties of gap-junction channels. For instance, a reduced sensitivity to transjunctional voltage has been reported for the Cx43–EGFP fusion protein [17]. However, molecularly engineered fluorescent tags are attractive tools for the study of Cx fate and function in gap-junction plaques [18].

In this study, we systematically compared the biophysical and permeability properties of wild-type human Cx26 and Cx30 transiently expressed in a clone of HeLa cells virtually devoid of connexins [19]. Cxs were inserted either as pIRES-EGFP constructs or as fusion proteins of the yellow (Cx26–EYFP, Cx30–EYFP) and cyan (Cx30–CFP) GFP mutants. As control, we employed the same HeLa cells stably transfected with mouse Cx26 [20]. Some of the present results have been presented in abstract form [21].

Materials and methods

Reagents. Alexa Fluor 488, Alexa Fluor 594, and calcein were purchased from Molecular Probes (Eugene, OR). Neurobiotin and 7-amino-4-methylcoumarin-3-acetic acid (AMCA)–streptavidin were from Vector Laboratories (Burlingame, CA). The polyclonal anti-rat Cx26 antibody employed was from Zymed Laboratories (San Francisco, CA). The secondary antibody was a tetramethylrhodamine isothiocyanate (TRITC)-conjugated affinity purified goat anti-rabbit IgG from Jackson ImmunoResearch Laboratories (West Grove, PA). All other reagents were from Sigma, unless otherwise specified.

Molecular cloning. The coding region of either wild-type human Cx26 (hCx26) or wild-type hCx30 was amplified from plasmids containing the cDNA, using primers containing *Xho*I and *Eco*RI recognition sequences. Purified products were subcloned into the corresponding sites of the bicistronic vector pIRES-EGFP (Clontech, Palo Alto, CA).

For fusion protein generation, the open reading frames (ORFs) of hCx26 and hCx30 were amplified by PCR using oligonucleotide primers that introduced *Eco*RI and *Bam*HI restriction enzyme sites at the 5′- and 3′-termini of the cDNAs, respectively, deleting the stop codon:

26for: 5′-CGGAATTCAGATGGATTGGGGCACG-3′
26rev: 5′-CGGGATCCACTGGCTTTTTTGACTT-3′
30for: 5′-CGGAATTCCCAGCGCAATGGATTGG-3′
30rev: 5′-CGGGATCCCTTGGGAAACCTGTGAT-3′

The resulting PCR products were digested with the two enzymes and ligated into the *Eco*RI–*Bam*HI sites of pEGFP-N1 (Clontech, Palo Alto, CA) followed by transformation into *Escherichia coli* (TOP10). Miniplasmid preparation and restriction enzyme analysis were performed to identify positive clones. All constructs were sequenced using the Dye Terminator (Perkin–Elmer, Wellesley, MA), as recommended by the manufacturer, to verify that PCR amplification did not introduce unwanted mutations.

Cell culture and transfection. A clone of HeLa cells essentially devoid of connexins [19] was provided by Prof. Klaus Willecke (University of Bonn, Germany) and cultured according to standard procedures. Cells were transfected with the expression vectors described above using the Lipofectamine transfection protocol (Gibco, Invitrogen, Leek, The Netherlands) 24 h after plating and experiments were performed 24 h after transfection. A clone of the same HeLa cells, stably expressing mCx26, the murine isoform of Cx26 (HeLa–Cx26) [20] was kindly provided by Prof. Marc Mesnil (University of Poitiers, France).

Intercellular dye transfer. Glass capillaries, prepared using a dual-step puller (Narishige, Tokyo, Japan), were filled with the following fluorescent dyes: lucifer yellow (LY, 5% solution in 0.33 M lithium chloride), Alexa Fluor 488 (10 mM solution in KCl 200 mM), calcein (2% solution in 0.15 M NaCl, 0.1 M $NaHCO_3$, pH 8.5), and Alexa Fluor 594 (10 mM solution in KCl 200 mM). For all dye transfer experiments, clusters of fluorescent cells were identified and single cells within the cluster perimeter were pressure-injected with a pneumatic PLI-100 pico-injector (Medical Systems, Greenvale, NY) mounted onto a Zeiss inverted Axiovert 100 TV microscope (Carl Zeiss, Jena, Germany). For GFP, LY, Alexa Fluor 488, and calcein, the filter set was Zeiss 09 (BP450-490/LP520). For Alexa Fluor 594, the filter set was Zeiss 15 (BP54612/LP590). Fluorescence images were collected through an oil immersion 40×, 1.8 NA objective, captured by a low light level CCD camera (Hamamatsu Photonics, Tokyo, Japan) and fed to a digital image processor developed in the laboratory. Intercellular diffusion of green/yellow dyes (GFP, LY, Alexa Fluor 488, and calcein) was monitored as described [10,15,16]. Following image processing, the number of injected cells that transferred the dye to more than one neighbour was scored. Subsequent processing was performed with Corel Photo-Paint (Corel, Ottawa, Canada) to generate false colour displays. For each dye, control experiments were performed by microinjecting non-transfected HeLa cells in the same dishes ($n = 80$). Neurobiotin (6% solution in 0.1 M Tris) was pressure-injected with a pneumatic PLI-100 pico-injector. Several cells were injected on each coverslip before quickly rinsing off the medium and fixing the cells in 4% paraformaldehyde for 30 min. Fixed cells were washed in PBS and permeabilized in PBS, supplemented with Triton X-100 0.1%, for 30 min. For neurobiotin recognition, AMCA–streptavidin (1 μg/ml solution in 0.15 M NaCl, 0.1 M $NaHCO_3$, pH 8.5) was incubated for 90 min. Following three 10-min washes in PBS, coverslips were mounted on glass slides and viewed under a Leica DMLS fluorescence microscope (Leica Microsystems, Wetzlar, Germany) through a 40× 0.65 NA objective. The GFP signal was visualized with a BP450–490/LP515 filter set, while AMCA fluorescence was visualized with a BP340–380/LP425 filter set. Cells were photographed with a Kodak Elitechrome 400 film (Eastman Kodak, Rochester, NY) with constant exposure times. Digital images from developed slides were obtained with a Polaroid SprintScan 4000 scanner (Polaroid, Waltham, MA). Images were stored digitally and exported to Corel Photo-Paint for reproduction.

Immunofluorescence and confocal microscopic analysis. All filters used in this study were purchased from Croma Technology (Bratlleboro, VT). HeLa–Cx26 cells and wild-type HeLa cells transfected with

relevant cDNA were grown onto glass coverslips and fixed with 2% paraformaldehyde. For immunofluorescence, the primary anti-Cx26 antibody and the secondary TRITC-conjugated antibody were incubated, respectively, for 1 h and for 30 min at 4 °C. Coverslips were mounted onto glass slides and visualized using a Bio-Rad 2100 MP confocal system (Bio-Rad, Hercules, CE) equipped with a Nikon objective (100×, 1.3 NA, Nikon, Tokyo, Japan), coupled to an upright microscope (ECLIPSE E600-FN, Nikon). When imaging EYFP or TRITC fluorescence, as described below, an auxiliary 2.6 magnification was applied, resulting in pixel size of 0.09 μm, and corresponding image area size of $47 \times 47\,\mu m^2$. In two controls, no signal was detected when using the secondary antibody alone.

To study gap-junction plaques with the use of Cx26 antibodies, HeLa cell pairs were transfected with hCx26 cDNA, subcloned into bicistronic pIRES-EGFP plasmid. Fluorescence emission from cytosolic EGFP and TRITC-conjugated antibodies was collected separately by sequential excitation of the sample with 488 and 543 nm argon laser lines, respectively, using standard filter sets (EGFP: dichroic 500DCLPXR, emission HQ515/30 band-pass filter; TRITC: dichroic HE570LP, no emission filter). For localization, images were processed and merged off line using the Bio-Rad Laser Sharp 2K 4.1 software.

Cells transfected with Cx26–EYFP chimeric constructs were illuminated by the 514-nm argon line, directed onto the sample by a Q515lpxru dichroic mirror, and visualized through a HQ545/40 band-pass emission filter. To obtain high-resolution images and three-dimensional volume reconstructions of gap junctions, a sequence of *z*-stack was captured at 0.4 μm steps covering a sample depth of 20 μm. Reconstructed volumes were subsequently rotated in software and viewed at an angle of 30° from the normal.

In separate experiments, the plasma membrane of HeLa cells transfected with hCx26–EYFP was stained with wheat germ agglutinin Texas red-X conjugated (TR, Molecular Probes). To reduce photo-bleaching of out of focus planes, simultaneous two-photon excitation of EYFP and TR fluorescence was promoted at 840 nm whilst separating emissions with narrow-band interference filters (525/35 nm for EYFP, 600/50 nm for TRITC). The auxiliary magnification for these experiments was 1.9×, yielding a pixel size of 0.13 μm and an image area size of $65 \times 65\,\mu m^2$. For volume reconstruction, *z*-stacks were collected at 0.2 μm steps, covering a sample depth of 22 μm. Finally, reconstructed volumes were viewed at an angle of 78° from the normal.

Dual patch clamp recordings. For electrophysiological recordings cells were grown on thin (No. 0) coverslips and transferred to an experimental chamber mounted on the stage of an upright microscope equipped with an infinity-corrected water-immersion objective (60×, 0.90 NA, LUMPlanFl, Olympus Optical, Tokyo, Japan). The bath solution contained (in mM) 137.7 NaCl, 5.4 KCl, 5 $CaCl_2$, 1 $MgCl_2$, 10 Hepes, 5 glucose, and 2 pyruvate, and pH was adjusted to 7.4 with NaOH (temperature 20–23 °C). Two List EPC-7 patch-clamp amplifiers (Heka Elektronik, Lambrecht/Pfalz, Germany) were selected to record electrical signals using patch-clamp pipettes formed on a vertical puller (PP-83, Narishige, Japan) from 1.5-mm o.d. soda glass (Harvard Apparatus, UK). Pipettes were filled with a solution containing (in mM): 120 K aspartate, 10 CsCl, 10 TEA Cl, 1 $MgCl_2$, 1 $CaCl_2$, 10 EGTA, 3 ATP, and adjusted to 7.2 with KOH and filtered through 0.22-μm pores. Pipette resistances were 3–5 MΩ when immersed in the bath. Current and voltage were sampled at rates between 1 and 20 kHz using a standard laboratory interface (1401*Plus*, Cambridge Electronic Design) controlled by software written in the laboratory. On average, the patch electrodes acquired an access resistance of 10–12 MΩ after patch break, whereas the input resistance of untransfected HeLa cells was >0.5 GΩ. To measure junctional conductance, each cell of a pair was voltage clamped independently with one of the two List amplifiers. By stepping the voltage in one cell (n.1) and keeping the other (n.2) constant, junctional current, I_j, was observed directly as a change in current in the unstepped cell (i.e., $I_j = -\Delta I_2$). When test voltages are applied to one cell (e.g., cell n.1), thus establishing a transjunctional voltage $V_j = V_1 - V_2$, current deflections ΔI_1 and ΔI_2, coincident in time and opposite in polarity, reflect changes in I_j. In several controls, weakly coupled cells, in which one or few gap-junctions channels were open at any time, exhibited equal-sized events of opposite polarity in each cell's current recording (mirror currents) [22]. Under these conditions, junctional conductance, g_j, was computed as I_j divided by V_j, corrected for the error due to the access resistance of both pipettes. The value of g_j was extremely variable from pair to pair. To measure accurately the voltage dependence of the normalized conductance $G_j = g_j / \max(g_j)$ on V_j, pairs coupled by conductances larger than 10 nS were discarded, thereby limiting the effect of series resistance on these measurements. To avoid interference with voltage-dependent gating when measuring tissue conductance, Tg_j, pulses of 10 mV amplitude were applied to one cell while the neighbouring cell was kept at a constant voltage near its resting potential. Between 10 and 15 Tg_j measurements, each one from a distinct cell pair, were made in each dish.

Results

Subcellular localization of connexins in transfected HeLa cells

Immunofluorescence performed with an anti-Cx26 antibody produced no signal in parental (communication incompetent), untransfected HeLa cells, but showed positive staining localized at cell–cell contact areas in a clone of HeLa cells stably transfected with mCx26 (not shown).

To compare the properties of murine (mCx26) and human Cx26 (hCx26), the coding region of wild-type (wt) hCx26 cDNA was subcloned into pIRES-EGFP and transiently expressed in parental HeLa cells [19]. The cellular localization of the hCx26 protein, analysed by immunofluorescence in EGFP positive cells (Fig. 1A, *top*), displayed dashed, membrane-associated staining typical of gap-junctional plaques (*middle*), indicating that hCx26wt was correctly targeted to the plasma membrane (*bottom*). Similar patterns were detected after expressing a chimeric protein formed by fusing hCx26 to EYFP, the yellow mutant of the GFP [21]. Parental HeLa cells transiently transfected with the Cx26–EYFP cDNA showed fluorescence puncta in the cytoplasm (Fig. 1B, *arrow heads*) and aggregation at the plasma membrane, particularly at contact points between two cells. To investigate the organization of these plaques and to reconstruct three-dimensional views of entire gap junctions, stacks of confocal sections were acquired (Figs. 1B and C) and the reconstructed volumes were visualized at different angles. The reconstructed structures resembled the junctional plaques viewed by immunofluorescence with Cx26-specific antibodies. Some plaques were rather large (Fig. 1B, *arrow*), often irregular, and in general characterized by long protrusions or deep invaginations, as previously reported [23]. Similar plaques were observed, after immunofluorescence, also in HeLa

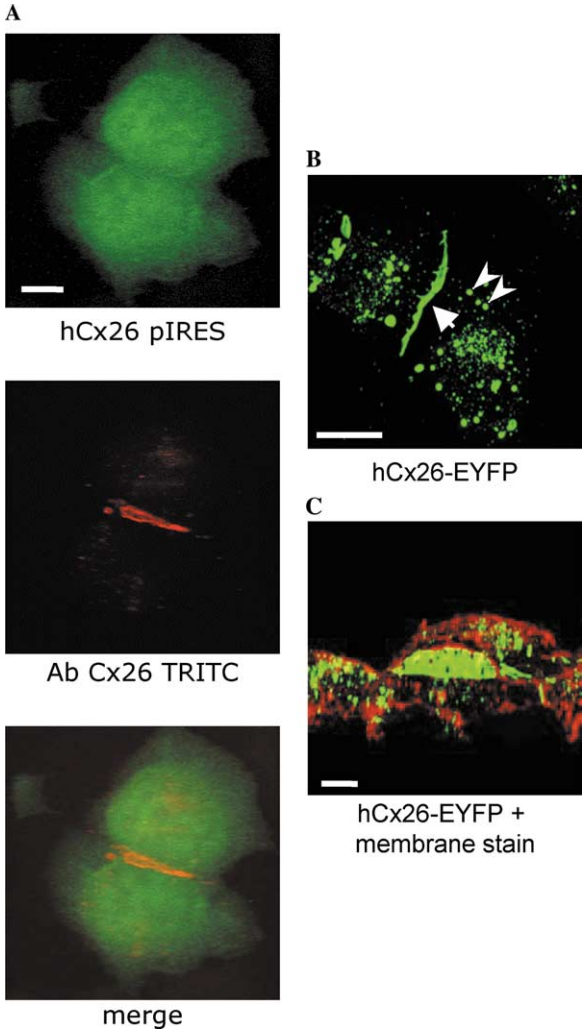

Fig. 1. Recombinant and chimeric connexins assemble into typical gap junctions when transiently transfected in communication-incompetent HeLa cells. (A) *Top*: Confocal fluorescence image of a representative HeLa cell pair transfected with the wild-type (wt) hCx26 cDNA subcloned into bicistronic pIRES-EGFP plasmid (Clontech). Diffuse fluorescence throughout the cell body due to EGFP was selected using a narrow-band green emission filter. *Middle*, the same confocal field viewed through a narrow-band red emission filtering, selecting fluorescence emission from a TRITC-conjugated anti-Cx26 antibody (Ab). *Bottom*: merge image obtained by assigning the top and middle panels to the green and red channels of an RGB picture, respectively. Note dashed, membrane-associated, staining localized at cell–cell contact areas typical of gap-junctional plaques and scattered fluorescence in the cytoplasm. (B) Confocal fluorescence image of a HeLa cell pair transfected with the hCx26–EYFP chimeric construct. The image was obtained from the volume reconstruction of a *z*-stack sequence captured at 0.4 μm intervals and viewed at an angle of 30° from the normal. *Arrow* and *arrow heads* indicate a representative junctional plaque and fluorescence puncta in the cytoplasm, respectively. (C) Same as B, for a different sample additionally stained with a membrane dye (Texas red, wheat germ agglutinin). This reconstructed volume was viewed at an angle of 78° from the normal, showing a large plaque in the adjoining plasma membranes of two neighbouring cells. Scale bars, 10 μm.

cells transfected with the pIRES-EGFP vector (data not shown). The expression level of the hCx26–EGFP fusion product varied considerably from cell to cell, as revealed by spots or thick lines at sites of cell-to-cell contact. Comparable expression levels and gap-junction plaque shapes were observed with hCx30, also fused to EYFP (data not shown).

Quantification of dye transfer efficiency

To analyse Cx26 permeability, five low molecular weight tracer molecules of different size and charges were microinjected into a single cell in a confluent culture. Intercellular dye transfer was considered positive when injected cells transferred the dye to more than one neighbour. Gap junctions between HeLa cells stably expressing mCx26 were permeable to all dyes up to MW 622, while the largest one, Alexa Fluor 594 (MW 759), failed to diffuse (Table 1). The intercellular transfer of dyes, assayed in clusters of parental HeLa cells transiently transfected with the pIRES-EGFP-hCx26wt vector, qualitatively confirmed the permeability properties observed for mCx26 in stable lines (Table 1). However, expression of hCx26-induced higher efficiency of dye transfer. Specifically, within 5 min of microinjecting a 622-MW dye in a single cell of a cluster, all other EGFP-positive cells in that cluster filled with this tracer, presumably diffusing through gap junctions. Interestingly, in 9 out of the 104 cases, the transfer of the larger Alexa Fluor 594 was also detected. In principle, these findings could either be the result of hCx26 overexpression, associated with transient transfection, or a characteristic feature of this gap-junction protein.

The possibility that channel permeability could be related to the level of Cx expression was explored by transient transfection of parental HeLa cells with the hCx26–EYFP fusion protein. Although GFP fusion to Cx43 apparently did not alter the permeability properties of this connexin [17,24], in those studies permeability analysis was limited to the smallest dyes available (neurobiotin and lucifer yellow). Consequently, the issue of a putative graded reduction of pore permeability remained unexplored. Here, we employed a wider panel of fluorescent tracers to examine the consequences of EYFP tagging on hCx26 permeability. The results are summarized in Table 1 and Fig. 2. The permeability of hCx26–EYFP to molecules up to MW 622 (calcein) was comparable to that of the non-tagged construct (transfected with the pIRES vector).The possibility of visually selecting cells that formed large plaques significantly increased the number of cells in which intercellular diffusion of Alexa Fluor 594 (MW 759) was detected in these measurements. These results indicate that channel permeability, at least when assessed in dye transfer experiments, is strictly related to connexin expression, and suggest that the cut-off dye size could be close to the exclusion limit of hCx26.

Table 1
Intercellular transfer of fluorescent dyes in HeLa cells stably expressing murine Cx26 (mCx26) or transiently transfected with human Cx26 and Cx30 (pIRES-EGFP and EYFP-tagged constructs)

Cx	Neurobiotin (MW 322 Da)	Lucifer yellow (MW 457 Da)	Alexa Fluor 488 (MW 570 Da)	Calcein (MW 622 Da)	Alexa Flour 594 (MW 759 Da)
mCx26	32 ($n = 40$)	10 ($n = 19$)	16 ($n = 21$)	12 ($n = 13$)	0 ($n = 20$)
hCx26 pIRES2-EGFP*	38 ($n = 40$)	83 ($n = 83$)	17 ($n = 17$)	32 ($n = 32$)	9 ($n = 104$)
hCx26–EYFP*	27 ($n = 40$)	49 ($n = 49$)	20 ($n = 20$)	21 ($n = 21$)	45 ($n = 67$)
hCx30 pIRES2-EGFP*	30 ($n = 40$)	3 ($n = 22$)			
hCx30–EGFP*	30 ($n = 35$)	13 ($n = 28$)			

* Communication-incompetent HeLa cells were transfected with the specified cDNA and analysed 24 h post-transfection. Individual cells in clusters expressing either cytosolic EGFP or membrane-associated EYFP were microinjected with the dyes specified above. Intercellular transfer was considered positive when the injected cell transferred the dye to more than one neighbour. *n*, total number of injections.

Fig. 2. Imaging intercellular transfer of membrane-impermeant dyes. HeLa cells were transfected with the hCx26–EYFP chimeric construct and analysed 24 h post-transfection. Individual cells in clusters expressing EYFP were microinjected with neurobiotin, lucifer yellow, Alexa Fluor 488, calcein, and Alexa Fluor 594. Intercellular diffusion of dyes was assessed 5 min after injection. *EYFP*: Clusters of EYFP-expressing cells before injection. *DYE*: Dye fluorescence (see Materials and methods). Scale bars, 10 μm.

Similar experiments were also performed on non-tagged hCx30 (pIRES-EGFP vector), as well as on the hCx30–EYFP fusion product. However, given the lower permeability reported for Cx30 channels [25], dye transfer analysis was limited to neurobiotin and lucifer yellow (Table 1). Permeability to neurobiotin was similar for tagged and non-tagged hCx30. Similar to the case of hCx26 reported above, also in these other experiments expression of the tagged protein increased the number of cells that permitted lucifer yellow to diffuse across a cluster.

Differences of tissue conductance values in stable lines and transient transfectants

In order to test for a possible correlation between dye transfer efficiency and electrical conductance, pairs of HeLa cells in physical contact to other cells in a cluster were subjected to dual patch-clamp measurements. Total intercellular conductance measured under these conditions provides an estimate of tissue conductance, Tg_j. While not accurate in an absolute sense due to non-junctional as well as membrane leak contributions, such measurements are nonetheless thought to reflect closely the relative levels of junctional conductance between clones [26], provided that cells to be compared are

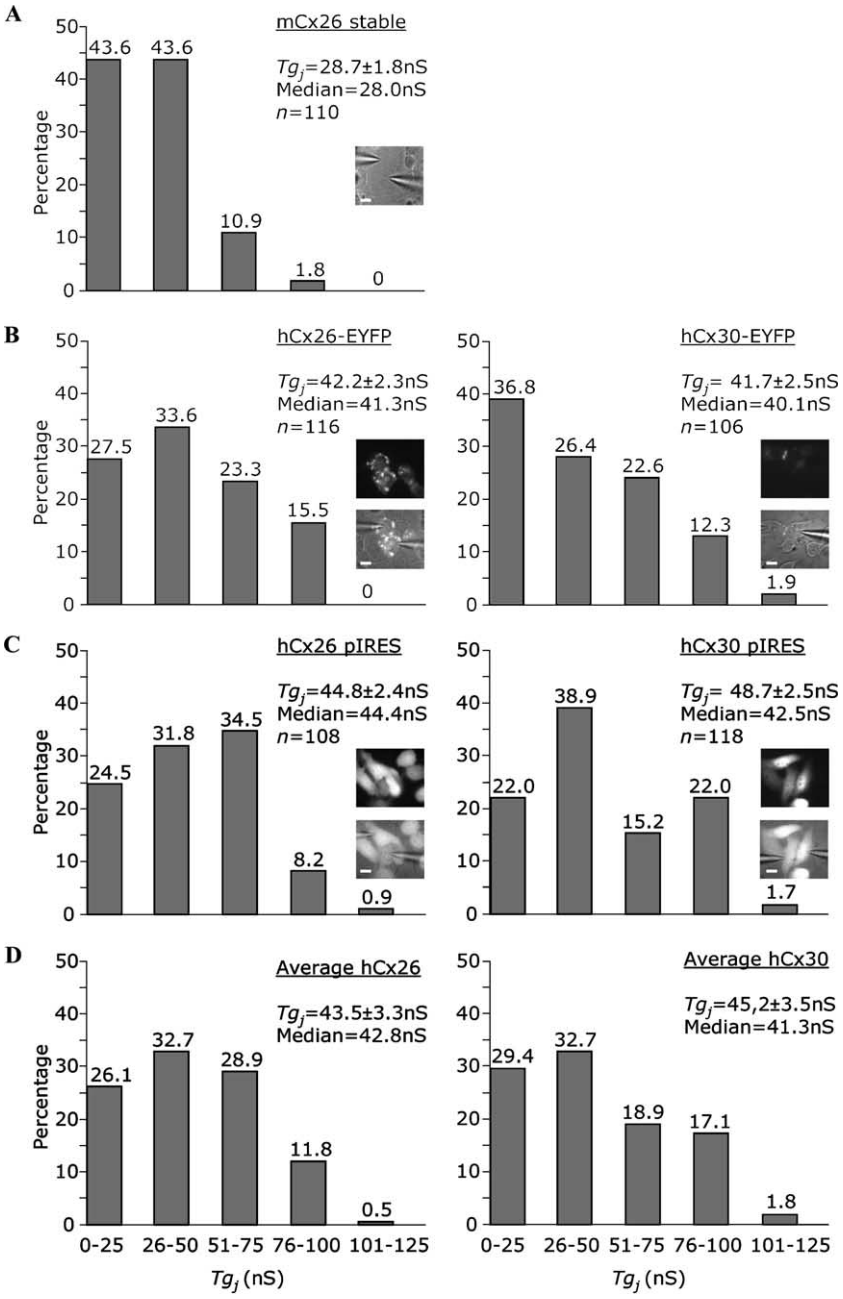

Fig. 3. Distribution of total intercellular conductance (Tg_j) in HeLa cells stably and transiently transfected with Cx26 and Cx30 constructs. (A) Stable line transfected with mCx26; *inset* shows bright field image of a representative cell pair in a cluster, with contacting patch electrodes. (B) Transient transfection with fusion products hCx26–EYFP (*left*) and hCx30 (*right*). (C) Transient transfection with bicistronic vector containing the cDNA of the EGFP together with hCx26 (*left*) and hCx30 (*right*). *Insets* in B and C are images obtained under epifluorescence illumination (*top*) and under combined bright field and epifluorescence illumination (*bottom*). (D) Pooled data obtained by combining the results shown in B and C for hCx26 (*left*) and hCx30 (*right*), respectively. Scale bars, 10 μm.

clonally related and of similar shape, size, packing density, and confluence. Fig. 3 shows the distribution of Tg_j for HeLa cells stably expressing mCx26 (A), those transiently transfected with the fusion products of EYFP to hCx26 and hCx30 (B), and with the corresponding non-tagged pIRES constructs (C). To try and poll a statistically representative population sample, each one of these five histograms was constructed using $n > 100$ distinct paired recordings. Hence, data pooled from panels (B and C) and shown in (D) have $n > 200$. Data analysis showed that hCx26 and hCx30 transfectants had very similar average Tg_j (median 42.8 nS, means $\pm$ SD $= 43.5 \pm 3.3$ nS for hCx26; median 41.3 nS, means $\pm$ SD $= 45.2 \pm 3.5$ nS for hCx30), whereas mCx26 stable lines displayed average Tg_j approximately 37% lower. This is essentially the result of a more skewed distribution of Tg_j for mCx26, in which the majority of coupling levels concentrated below 50 nS.

Voltage dependence of gap-junction conductance of murine Cx26, human Cx26, and Cx30

The above values likely reflect differences in the expression level of stably transfected mCx26, on the one hand, and transiently transfect hCx26 and 30, on the other hand. To ascertain whether these differences also depended on intrinsic properties of the gap-junction channels, we carried out a more detailed analysis of conductance properties by applying the dual patch-clamp recording technique to isolated cell pairs (Fig. 4). The voltage dependence of normalized junctional conductance, G_j, on transjunctional voltage, V_j, was assessed using voltage steps (Figs. 4A and C) or slow ramps (Figs. 4B, D, and E). When applied to non-tagged hCx26 constructs (Fig. 4C) and to EYFP–hCx26 fusion products (Fig. 4D), both techniques gave very similar results, indicating that (i) steps and slow ramps can be

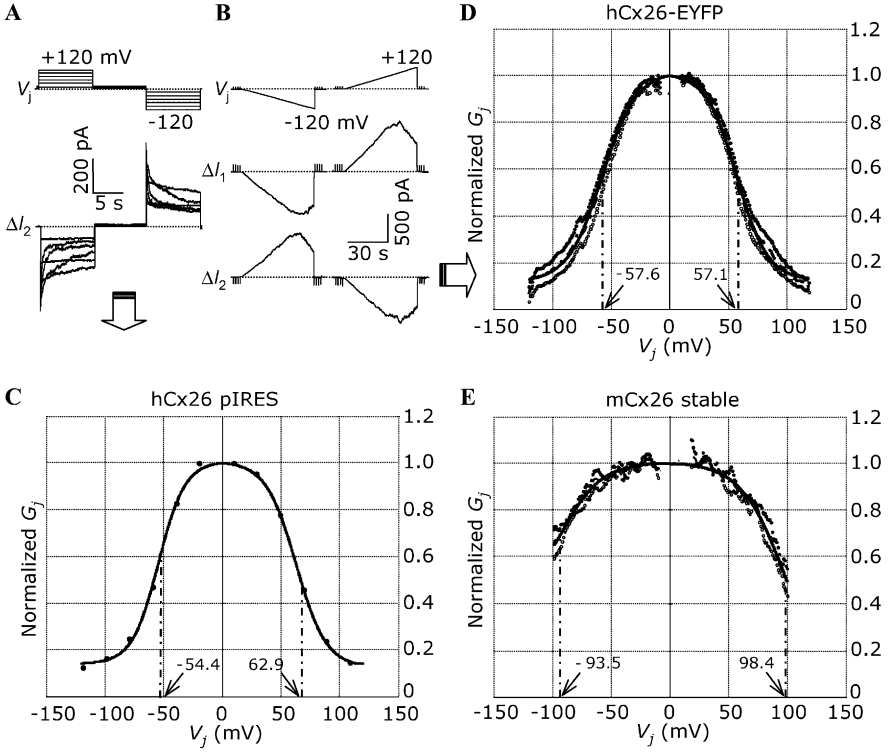

Fig. 4. Voltage dependence of gap-junction conductance in isolated HeLa cell pairs stably and transiently transfected with Cx26 and Cx30 constructs. (A) *Top*: Voltage commands applied to one of two neighbouring cells (conventionally, cell 1), each one separately patch-clamped with a different amplifier; *bottom*: junctional currents recorded from the adjacent cell (cell 2), which was kept at the common pre-stimulus holding potential (−20 mV). Cells in A were transiently transfected with hCx26 cDNA hosted in a bicistronic vector that also carried the cDNA of EGFP. Dotted lines indicate pre-stimulus values of voltage and current, from which differences (V_j, ΔI_2) were measured to compute junctional conductance. (B) *Top*: Voltage ramps applied to cell 1 in a culture stably transfected with mCx26; *bottom*: whole cell currents recorded simultaneously from cell 1 and the adjacent cell 2, which was kept at the common pre-stimulus holding potential (−20 mV). Dotted lines indicate pre-stimulus values of voltage and current, from which differences (V_j, $\Delta I_1, \Delta I_2$) were measured to compute junctional conductance. (C) Normalized conductance G_j (*circles*) vs. transjunctional potential V_j (*abscissa*) from steady-state data in A (currents measured 10 ms before the end of each voltage step). (D) Normalized conductance (*ordinates*) vs. transjunctional voltage (*abscissa*) measured from ramp responses in cell pairs transiently transfected with the fusion product hCx26–EYFP: mean (*squares*), minima (*open circles*), and maxima (*closed circles*) of $n = 25$ pairs. (E) Same as D for pairs stably transfected with mCx26 ($n = 2$). Arrows in C–E point to the values of the half-inactivation voltages V_0 derived by fitting the data with offset and scaled Boltzmann functions (*solid lines*). Fit parameters are provided in Table 2. The same ramp protocol shown in B was applied to all recordings used to construct plots in D and E.

used interchangeably for these recordings [27] and (ii) fusion to EYFP did not appreciably affect the voltage sensitivity of hCx26. However, comparing these results to ramp responses obtained from stable lines (Fig. 4E) did highlight a hitherto unreported, and unexpected, augmented voltage sensitivity of the human protein relative its murine counterpart [28].

This type of analysis was extended to the hCx30–EYFP fusion product (Fig. 5A), as well as to a construct similarly obtained by fusing hCx30 to the cyan mutant (*bottom*) of the GFP (CFP). Again, the similarity of the bell-shaped curves obtained from these two chimeras, which are also similar to previously published data obtained from their murine counterpart in the same expression systems [29], indicates that the fluorescent protein tags did not interfere with the voltage-gating properties of hCx30. G_j vs. V_j relationships shown in Figs. 4 and 5 were fitted by Boltzmann curves (*solid lines*) whose parameters are reported in Table 2. Fits to data in Figs. 4D and E and Fig. 5A are shown superimposed in Fig. 5C for ease of comparison.

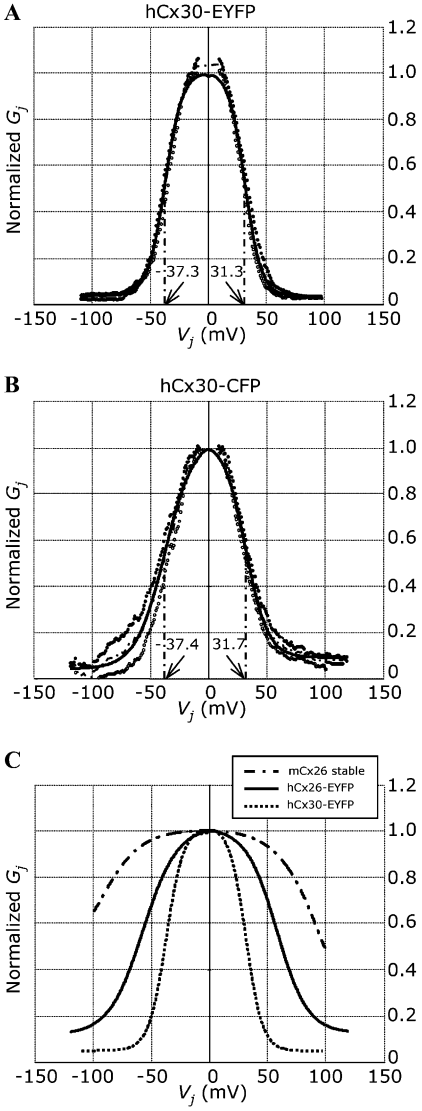

Fig. 5. Voltage dependence of gap-junction conductance in isolated HeLa cell pairs transiently transfected with hCx30 fusion proteins. (A) Normalized conductance (*ordinates*) vs. transjunctional voltage (*abscissa*) of hCx30–EYFP: mean (*squares*), minimum (*open circles*), and maxima (*closed circles*) of $n = 3$ pairs. (B) Same as A for hCx30–CFP ($n = 11$). Arrows in A and B point to the values of the half-inactivation voltages V_0 derived by fitting the data with offset and scaled Boltzmann functions (*solid lines*). Fit parameters are provided in Table 2. Ramp protocol as in Fig. 4. (C) Comparing Boltzmann fits to mCx26 (*dashed–dotted line*), hCx26–EYFP (*solid line*), and hCx30–CFP (*dotted line*) (data from panels D and E of Fig. 4, and A of this figure).

Table 2
Boltzmann fit parameters for normalized junctional conductance, G_j, measured in HeLa cells stably expressing murine Cx26 (mCx26), or transiently transfected with human Cx26 and Cx30 using EYFP-tagged constructs as well as non-tagged pIRES-EGFP bicistronic vectors

Connexin	V_j polarity	G_j max	G_j min	z	V_0 (mV)
mCx26	+	1	0.02	1.3	98.4
Stable line	−	1	0.38	1.4	93.5
hCx26 pIRES-EGFP	+	1	0.12	1.9	62.9
Bicistronic vector	−	1	0.14	2.8	54.4
hCx26–EYFP	+	1	0.12	1.9	57.1
Fusion product	−	1	0.12	1.7	57.6
hCx30–EYFP	+	1	0.04	3.6	31.3
Fusion product	−	1	0.04	3.4	37.3
hCx30–CFP	+	1	0.09	2.7	31.7
Fusion product	−	1	0.04	2.0	37.4

Discussion and conclusions

Connexin functional studies have been carried out in expression system by reconstituting gap-junction communication either by microinjecting cRNAs in *Xenopus laevis* oocytes [15,16,30] or by transfecting mammalian cells devoid of endogenous connexins with relevant cDNAs [9–16].

The construction of expression vectors that allow the identification of transfected cells by means of a co-expressed fluorescent reporter (e.g., the enhanced green fluorescent protein—EGFP) has been recently employed in the rapid and efficient functional-analysis screening of several Cx26, Cx30, and Cx31 missense mutations [10,12,13,15,16]. Some of these mutations have been reported to cause genetic deafness and, in selected cases, have been subjected to functionality tests [9–16,30].

The systematic comparison of the biophysical properties of human Cx26 and Cx30 conducted here indicates that, when properly linked, fluorescent protein tags based on GFP colour mutants do not alter appreciably gating or permeability of these connexins.

Therefore these fusion products seem reasonable candidate tools for functional studies, particularly those addressing the consequences of connexin mutations involved in genetic diseases. Moreover, the possibility of selecting junctional plaques of comparable size permits an indirect normalization for recombinant Cx expression level, and thus appears helpful in defining the limiting size of exchangeable molecules for each connexin. Finally, the increased voltage sensitivity of human Cx26 relative to its murine counterpart reported here might underlie important species-specific functional differences, which may be particularly relevant for the auditory system.

Acknowledgments

This work was supported by Grants from Telethon (Grant GGP02043), MIUR-PRIN 2002, and MIUR-FIRB 2001 (F.M. and P.D'A.), Regione Friuli Venezia-Giulia (P.D'A.) and INFM TSSEBB2 (F.M.). We thank Sabina Morassutto for assistance, Roberto Bruzzone (Institut Pasteur, Paris, France) for hCx26 and Cx30 cDNAs, and Klaus Willecke (University of Bonn, Germany) and Marc Mesnil (University of Poitieres, France) for the generous gift of the communication-incompetent and mCx26 expressing HeLa clones, respectively.

References

[1] J. Bergoffen, S.S. Scherer, S. Wang, M. Oronzi Scott, L.J. Bone, D.L. Paul, K. Chen, M.W. Lensch, P.F. Chance, K.H. Fischbeck, Connexin mutations in X-linked Charcot–Marie–Tooth disease, Science 262 (1993) 2039–2042.

[2] A. Shiels, D. Mackay, A. Ionides, V. Berry, A. Moore, S. Bhattacharya, A missense mutation in the human connexin50 gene (GJA8) underlies autosomal dominant "zonular pulverulent" cataract, on chromosome 1q, Am. J. Hum. Genet. 62 (1998) 526–532.

[3] D. Mackay, A. Ionides, Z. Kibar, G. Rouleau, V. Berry, A. Moore, A. Shiels, S. Bhattacharya, Connexin46 mutations in autosomal dominant congenital cataract, Am. J. Hum. Genet. 64 (1999) 1357–1364.

[4] D.P. Kelsell, J. Dunlop, H.P. Stevens, H.J. Lench, J.N. Liang, G. Parry, R.F. Mueller, I.M. Leigh, Cx26 mutations in hereditary non-syndromic sensorineural deafness, Nature 387 (1997) 80–83.

[5] A. Grifa, C.A. Wagner, L. D'Ambrosio, S. Melchionda, F. Bernardi, N. Lopez-Bigas, et al., Mutations in GJB6 cause nonsyndromic autosomal dominant deafness at DFNA3 locus, Nat. Genet. 23 (1999) 16–18.

[6] G. Richard, L.E. Smith, R.A. Bailey, P. Itin, D. Hohl, E.H. Epstein Jr., et al., Mutations in the human Cx gene GJB3 cause erythrokeratodermia variabilis, Nat. Genet. 20 (1998) 366–369.

[7] J. Xia, C. Liu, B. Tang, Q. Pan, L. Huang, H. Dai, et al., Mutations in the gene encoding gap junction protein β-3 associated with autosomal dominant hearing impairment, Nat. Genet. 20 (1998) 370–373.

[8] J. Lamartine, G. Munhoz Essenfelder, Z. Kibar, I. Lanneluc, E. Callouet, D. Laoudj, G. Lemaitre, Mutations in GJB6 cause hidrotic ectodermal dysplasia, Nat. Genet. 26 (2000) 142–144.

[9] P.E.M. Martin, S.L. Colbam, S.O. Casalotti, A. Forge, W.H. Evans, Properties of connexin26 gap junctional proteins derived from mutations associated with non-syndromal hereditary deafness, Hum. Mol. Gen. 8 (1999) 2369–2376.

[10] P. D'Andrea, V. Veronesi, M. Bicego, S. Melchionda, L. Zelante, E. Di Iorio, R. Bruzzone, P. Gasparini, Hearing loss: frequency and functional studies of the most common connexin26 alleles, Biochem. Biophys. Res. Commun. 296 (2002) 685–691.

[11] E. Thonnissen, R. Rabionet, M.L. Arbones, X. Estivill, K. Willecke, T. Ott, Human connexin26 (GJB2) deafness mutations affect the function of gap junction channels at different levels of protein expression, Hum. Genet. 111 (2002) 190–197.

[12] J.E. Common, D. Becker, W.L. Di, I.M. Leigh, E.A. O'Toole, D.P. Kelsell, Functional studies of human skin disease- and deafness-associated connexin 30 mutations, Biochem. Biophys. Res. Commun. 298 (2002) 651–656.

[13] W.L. Di, J. Monypenny, J.E. Common, C.T. Kennedy, K.A. Holland, I.M. Leigh, E.L. Rugg, D. Zicha, D.P. Kelsell, Defective trafficking and cell death is characteristic of skin disease-associated connexin 31 mutations, Hum Mol Genet. 11 (2002) 2005–2014.

[14] A. Oshima, T. Doi, K. Mitsuoka, S. Maeda, Y. Fujiyoshi, Roles of Met-34, Cys-64, and Arg-75 in the assembly of human connexin 26. Implication for key amino acid residues for channel formation and function, J. Biol. Chem. 278 (2003) 1807–1816.

[15] R. Bruzzone, D. Gomes, E. Denoyelle, N. Duval, J. Perea, V. Veronesi, D. Weil, C. Petit, M.M. Gabellec, P. D'Andrea, T.W. White, Functional analysis of a dominant mutation of human connexin26 associated with nonsyndromic deafness, Cell Commun. Adhes. 8 (2001) 425–431.

[16] R. Bruzzone, D. Gomès, V. Veronesi, M. Bicego, C. Petit, N. Duval, P. D'Andrea, T.W. White, Functional analysis of recessive mutations of human connexin26 associated with nonsyndromic deafness, FEBS Lett. 533 (2003) 59–88.

[17] F.F. Bukauskas, K. Jordan, A. Bukauskiene, M.V. Bennett, P.D. Lampe, D.W. Laird, V.K. Verselis, Clustering of connexin 43-enhanced green fluorescent protein gap junction channels and functional coupling in living cells, Proc. Natl. Acad. Sci. USA 97 (2000) 2556–2561.

[18] V.K. Verselis, F. Bukauskas, Connexin-GFPs shed light on regulation of cell–cell communication by gap junctions, Curr. Drug Targets 3 (2002) 483–499.

[19] C. Elfgang, R. Eckert, H. Lichtenberg-Fraté, A. Butterweck, O. Traub, R.A. Klein, D.F. Hülser, K. Willecke, Specific permeability and selective formation of gap junction channels in Cx-transfected HeLa cells, J. Cell Biol. 129 (1995) 805–817.

[20] M. Mesnil, V. Krutovskikh, C. Piccoli, C. Elfgang, O. Traub, K. Willecke, H. Yamasaki, Negative growth control of HeLa cells by connexin genes: connexin species specificity, Cancer Res. 55 (1995) 629–639.

[21] M. Beltramello, V. Piazza, F. Mammano, Membrane targeting and voltage gating of connexin 26 and 30 fused to GFP colour variants, J. Physiol. 544.P (2002) 12–13.

[22] J. Neyton, A. Trautmann, Single-channel currents of an intercellular junction, Nature 317 (1985) 331–335.

[23] M.M. Falk, Connexin-specific distribution within gap junctions revealed in living cells, J. Cell Sci. 113 (2000) 4109–4120.

[24] K. Jordan, J.L. Solan, M. Dominguez, M. Sia, A. Hand, P.D. Lampe, D.W. Laird, Trafficking, assembly, and function of a connexin43-green fluorescent protein chimera in live mammalian cells, Mol. Biol. Cell. 10 (1999) 2033–2050.

[25] D. Manthey, K. Banach, T. Desplantez, C.G. Lee, C.A. Kozak, O. Traub, R. Weingart, K. Willecke, Intracellular domains of mouse connexin26 and -30 affect diffusional and electrical properties of gap junction channels, J. Membr. Biol. 18 (2001) 137–148.

[26] F. Cao, R. Eckert, C. Elfgang, J.M. Nitsche, S.A. Snyder, D.F. Hülser, K. Willecke, B.J. Nicholson, A quantitative analysis of

connexin-specific permeability differences of gap junctions expressed in HeLa transfectants and *Xenopus oocytes*, J. Cell Sci. 111 (1998) 31–43.

[27] R.D. Veenstra, Voltage clamp limitations of dual whole-cell gap junction current and voltage recordings. I. Conductance measurements, Biophys. J. 80 (2001) 2231–2247.

[28] V. Valiunas, H. Niessen, K. Willecke, R. Weingart, Electrophysiological properties of gap junction channels in hepatocytes isolated from connexin32-deficient and wild-type mice, Pflug. Arch. 437 (1999) 846–856.

[29] V. Valiunas, D. Manthey, R. Vogel, K. Willecke, R. Weingart, Biophysical properties of mouse connexin30 gap junction channels studied in transfected human HeLa cells, J. Physiol. 519 (1999) 631–644.

[30] T.W. White, M.R. Deans, D.P. Kelsell, D.L. Paul, Connexin mutations in deafness, Nature 394 (1998) 630–631.